The Effects of Radiation and MHD Casson Nanofluid Darcy Forchheimer Flow on an Inclined Plate with Chemical Reactions: Biomedical Applications

M. Sreedhar Babu[1], P. Naga Raju[2], B. Mallikarjuna Reddy[3]

[1]*Department of Applied Mathematics, Yogi Vemana University, Kadapa, Andhra Pradesh, India.*
[2]*Department of Applied Mathematics, Yogi Vemana University, Kadapa, Andhra Pradesh, India.*
[3]*Department of Applied Mathematics, Yogi Vemana University, Kadapa, Andhra Pradesh, India.*
** Corresponding author E-mail: chinna20021996@gmail.com*

Article History: Received: 20-05-2023 **Revised:** 17-06-2023 **Accepted:** 07-07-2023

ABSTRACT

This inquiry examines the steady-state chemical reaction, thermal radiation, and MHD Casson nanofluid (Blood /copper (Cu)) buoyancy-driven Darcy Forchheimer flow over an inclined plate. PDEs are converted into nonlinear ODEs through the similarity method. The Runge-Kutta fourth-order approach is used to numerically solve these equations using Maple software. Velocity, Temperature, and concentration profiles have been studied about the effects of the magnetic field, porosity, buoyancy force parameter, velocity, temperature, concentration slips, thermal radiation, chemical reaction, thermophoresis, and Schmidt number. There are also Nusselt and Skin Friction Sherwood numbers. A table and a graph are used to display the computed results. The velocity profile decreases for Non-Newtonian fluid and Newtonian fluid over inclined plates while the porosity and magnetic field parameters increase. As the standards of the magnetic field, thermal radiation, and volume friction increase, the temperature increases in cases of Newtonian and non-Newtonian fluids. As the chemical reaction parameters rise, inclined plate concentration profiles increase for Non-Newtonian fluid and Newtonian fluid. As the Sherwood number and Nusselt number across an inclined plate increase, the impression of radiation, and magnetic field values seems to be growing. It is used extensively in biomedicine for antibacterial, diagnostic, and medication delivery purposes.

KEYWORDS MHD, thermal radiation, chemical reaction, thermophoresis, Darcy Forchheimer.

DOI: 10.48047/ecb/2023.12.Si8.658

1. Introduction

A nanofluid is a diluted suspension of sub-nanometer-sized solid atoms in a base fluid like water, oil, or ethylene glycol (Cu, Al, Ag, etc.). By using the improved thermal conductivity and stability offered by nanofluids, new types of stable suspensions may be produced. Convective transport models for nanofluids have been developed as a consequence of the work of several researchers. Researchers have investigated a non-homogeneous model using nanofluids for probing convective transport processes and seven-slip mechanisms. Due to their unique properties, nanofluids have the potential to be useful in a variety of heat transfer applications, including heat exchangers, microelectronics, pharmaceutical operations, automotive cooling, and hybrid engines. Many researchers have been interested in nanofluid in recent years because it has higher thermal conductivity than base fluids, which are vital for heat transfer. Nanofluids, a stable suspension of a base liquid and nanoparticles, were initially described by .) Choi [1]. Najma Ahmed et al. [2] explored the transient MHD convective flow of fractional nanofluid across vertical plates. The consequences of MHD human blood flows in nanofluids were explored by Khan et al [3]. Hayat et al [4] explored the MHD flow of nanofluids over a curved Surface.

To accurately predict the complicated boundary layer flow characteristics is the major objective of boundary layer study. A lot of researchers that focus on boundary layers and heat transfer have considered delving into this subject. A flat plate that was either horizontal or inclined was recommended in some research on the topic, although others recommended using a vertical plate. investigating boundary layers, heat, mass transfer, extruding plastic sheets, including die-extruded polymer sheets, continuous casting, spinning fibers from glass blowing, etc. The MHD hybrid nanofluids were investigated across a perpendicular plate by Khan et al. [5]. Badruddin et al. [6] show how heat radiation and porous media affect a vertical plate. The impact of dusty slip flows through an SCNT-MCNT over an endlessly inclined plate was studied by [7]. several researchers addressed the inclined and flat plates [8]–[10].

Researchers in many fields of technology and science, including nuclear engineering, have paid close attention to the problems with magnetohydrodynamic (MHD) natural convective flow.

industrial processes in material processing, industrial processes in metallurgy, pumps, accelerators, generators, and plasma jet engines. Raghunath [11] has investigated how an MHD hybrid nanofluid flow transports heat over a stretched sheet. Sudarsana Reddy et al [12] investigate the influence of magnetic fields, and heat generation on the flow of a nanofluid across a plate with a porous medium. The MHD flow of a nanofluid across an inclined plate was studied by Goyal et al.[13]. several researchers addressed the MHD.[14]–[19].

The characteristics of the electromagnetic energy that a material produces as a function of its heat are explained by thermal radiation, and temperature impacts these qualities. Thermal radiation increases thermal diffusivity and allows heat to be released. Thermal radiation is often used in industrial and high-temperature applications, solar panels, and nuclear power plants, as well as in the production of food, energy, missiles, gas turbines, aerospace engineering, and pharmaceuticals. Shafiq et al. [20] examined the influence of MHD micropolar fluid flow on the inclined sheet. Gulle et al. [21] deliberated the effects of radiation and MHD Jeffrey fluid flow on the inclined porous plate. Maghsoudi et al. [22] examined the result of non-Newtonian fluid on thermal radiation flow through an infinity of vertical flat plates.[23]–[27]

If it exists, a porous material or substance is porous. Porous media are present in biological tissues, rocks, the ground, sand, and wooden structures since they are all made of natural materials. Modifications to this material usually make use of its porosity. For example, porous media have many uses in thermal insulation, including geothermal systems, such as flesh extra and biomedical applications, which has aroused the attention of researchers and academics to carry out more research. The MHD flows of mixed nanofluid crossways in a porous Plate were investigated by Barik et al. [28]. Hydromagnetic free convection flows via an infinite plate in a porous media are studied by Bang Sarma et al. [29]. Many researchers are discussed by Puros Medium.[27], [30], [31].

This study of MHD Casson nanofluid (Blood/Cu) flows over a porous inclined plate with computation of Newtonian and non-Newtonian fluids. The numerical method (RK 4th order Method) in the Maple program is used to solve coupled nonlinear PDEs that are converted into ODEs using self-similarity. The impacts of so many effects of the porosity, Darcy Forchheimer, magnetic field, heat generation, buoyancy parameter, slip conditions parameters, thermal radiation, Schmidt number, and thermophoresis parameters on temperature, velocity, and concentration profiles have been examined. Nusselt number, Skin friction, and Sherwood number are also included. The computed results are shown explicitly and in a table. It is used extensively in biomedicine for antibacterial, diagnostic, and medication delivery purposes.

2. Formulation in mathematics

Consider an incompressible, steady, 2D modal, and Magnetohydrodynamic MHD Casson nanofluid flow which includes the significance over an inclined permeable plate. We employed Blood as the basis fluid and copper (*Cu*) nanoparticles. A magnetic field of uniform intensity B_0 is provided in the y-direction, which is usual to the flow direction, with the x-axis measured along the plate. External flow has a constant velocity U_∞ and occurs in a direction parallel to the slanted plate. The plate is maintained at a constant temperature T_w whereas the ambient temperature T_∞ where $T_w > T_\infty$. The plate and ambient species concentrations as C_w and C_∞ are considered.

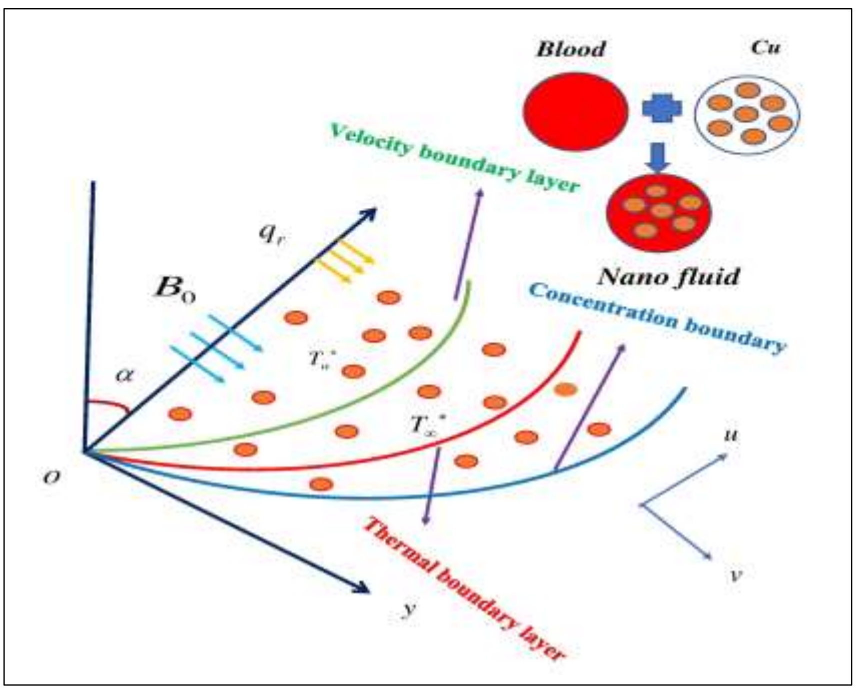

Fig 1. Nanofluid flow diagram with inclined plates.

The modal's flow diagram is shown in Fig. 1. We are investigating the impacts of MHD, radiation, Joule heating, porous material, and slips condition. Thermophoresis is considered to get a precise look at the mass deposit on the plate's surface. The following equations explain flows of continuity, momentum, or energy:[32]–[34]. Casson fluid rheological model equation satisfies Das et al. [15] and Krishnart al. [35].

$$\tau = \tau_0 + \mu\beta^*$$

Equivalently

$$\tau_{ij} = \begin{cases} \left(\mu_B + \dfrac{p_y}{\sqrt{2\pi}}\right) 2e_{ij} & when \;\; \pi > \pi_c \;, \\ \left(\mu_B + \dfrac{p_y}{\sqrt{2\pi_c}}\right) 2e_{ij} & when \;\; \pi < \pi_c \end{cases} \tag{1}$$

Here τ , α^* , μ , τ_0 , and are shear stress, shear rate, dynamic viscosity, and Casson yield stress, and $\pi = e_{ij}e_{ij}$ and eij is the (i,j)th a factor affecting the rate of deformation, π is the non-Newtonian fluid-based product, π_c is this product's essential value, the fluid's non-Newtonian non-plastic dynamic viscosity is μ_B and p_y yield stress of the fluid. Casson fluid basic rheological equations are as follows:

$$\tau_{ij} = \mu_B \left(1 + \frac{1}{\beta}\right) 2e_{ij} \tag{2}$$

Where $\beta = \mu_B \dfrac{\sqrt{2\pi}}{p_y}$, When $\beta \to \infty$ the fluid is non-Newtonian behavior disappears and it functions much like a Newtonian fluid.

$$\frac{\partial u}{\partial x}+\frac{\partial v}{\partial y}=0 \tag{3}$$

$$\begin{aligned}\rho_{nf}\left(u\frac{\partial u}{\partial x}+v\frac{\partial u}{\partial y}\right)&=\mu_{nf}\left(1+\frac{1}{\beta}\right)\frac{\partial^2 u}{\partial y^2}+\cos\alpha\left[g\left(\rho\beta_1\right)_{nf}\left(T-T_\infty\right)+g\left(\rho\beta_2\right)_{nf}\left(T-T_\infty\right)^2\right]\\&+\cos\alpha\left[g\left(\rho\beta_1^*\right)_{nf}\left(C-C_\infty\right)+g\left(\rho\beta_2^*\right)_{nf}\left(C-C_\infty\right)^2\right]-\sigma_{nf}B_0^2u-\mu_{nf}\frac{u}{k_1}-Fu^2\end{aligned} \tag{4}$$

$$u\frac{\partial T}{\partial x}+v\frac{\partial T}{\partial y}=\frac{k_{nf}}{(\rho c_p)_{nf}}\left(\frac{\partial^2 T}{\partial y^2}\right)-\frac{1}{(\rho c_p)_{nf}}\frac{\partial q_r}{\partial y}+\frac{\mu_{nf}}{(\rho c_p)_{nf}}\left(1+\frac{1}{\beta}\right)\left(\frac{\partial u}{\partial y}\right)^2+\frac{\sigma_{nf}}{(\rho c_p)_{nf}}B_0^2u^2+\frac{Q_o}{(\rho c_p)_{nf}}(T-T_\infty) \tag{5}$$

$$u\frac{\partial C}{\partial x}+v\frac{\partial C}{\partial y}=D\left(\frac{\partial^2 C}{\partial y^2}\right)-\frac{\partial V_T C}{\partial y}-Kr\left(C-C_\infty\right)^n \tag{6}$$

Boundary conditions

$$\left.\begin{array}{ll}v=\pm v_w(x),\quad u=U_0+L_2\left(1+\dfrac{1}{\beta}\right)\dfrac{\partial u}{\partial y}\ ,\quad T=T_w+L_1\dfrac{\partial T}{\partial y},\quad C=C_w+L_3\dfrac{\partial C}{\partial y}=0 & as\quad y\to 0\\ u=0,\qquad T=T_\infty,\qquad C=C_\infty & as\quad y\to\infty.\end{array}\right\} \tag{7}$$

Thermophysical nanofluid models are as follows:

$$\begin{aligned}&\mu_{nf}=\frac{\mu_f}{\left(1-\phi_1\right)^{2.5}},\alpha_{nf}=\frac{k_{nf}}{(\rho c_p)_{nf}},\upsilon_{nf}=\frac{\mu_{nf}}{\rho_{nf}}.\\&.\quad \rho_{nf}=\left(1-\phi\right)\rho_f+\rho_s\phi\\&(\rho C_p)_{nf}=\left(1-\phi\right)(\rho c_p)_f+\phi(\rho c_p)_s\\&(\rho\beta)_{nf}=\left(1-\phi\right)(\rho\beta)_f+\phi(\rho\beta)_s\end{aligned} \tag{8}$$

$$\frac{\sigma_{nf}}{\sigma_f}=1+\frac{3\left(\dfrac{\sigma_s}{\sigma_f}-1\right)\phi}{\left(\dfrac{\sigma_s}{\sigma_f}+2\right)-\left(\dfrac{\sigma_s}{\sigma_f}-1\right)\phi}\text{ and }k_{nf}=\left[\frac{k_s+2k_f-2\phi\left(k_f-k_s\right)}{k_s+2k_f+\phi\left(k_f-k_s\right)}\right]k_f$$

The following similarity transmutations are considered:

$$\eta=y\sqrt{\frac{U_0}{2\nu x}},\ \theta(\eta)=\frac{T-T_\infty}{T_w-T_\infty},\psi=\sqrt{2\nu xU_0}\,f(\eta),\ \phi(\eta)=\frac{C-C_\infty}{C_w-C_\infty} \tag{9}$$

Steam flows as it flows.

$$u = \frac{\partial \psi}{\partial y} \text{ and } v = -\frac{\partial \psi}{\partial x} \tag{10}$$

$$u = U_0 f'(\eta) \text{ and } v = -\sqrt{\frac{\nu U_0}{2x}}\left(f - \eta f'\right) \tag{11}$$

Substituting Equations (9) and (11) into Equations (4) – (7) gives

$$A_1\left(1+\frac{1}{\beta}\right) f''' + A_2 ff'' + A_6 \gamma \cos\alpha \left(\theta + \delta_1 \theta^2 + N(\phi + \delta_1 \phi^2)\right) - A_1 K\ f' - A_3 M\ f' - Fr\left(f'\right)^2 = 0 \tag{12}$$

$$\left(A_5 + Rd\right)\theta'' + A_4 \Pr f\theta' + A_1 \Pr Ec\left(1+\frac{1}{\beta}\right) f''^2 + A_3 \Pr EcM\left(f'\right)^2 + Q\Pr\theta = 0 \tag{13}$$

$$\phi'' + Scf\phi' - Sc\tau\theta'\phi' - Sc\tau\phi\theta'' - Sc\gamma_1\phi^n = 0 \tag{14}$$

Boundary condition

$$\left.\begin{aligned} & f'(0) = 1 + D_1\left(1+\frac{1}{\beta}\right) f''(0), \quad f(0) = S, \quad \theta(0) = 1 + D_2\ \theta'(0), \quad \phi(0) = 1 + D_2\ \phi'(0) \\ & f'(\infty) = 0, \quad \theta(\infty) = 0, \quad \phi(\infty) = 0. \end{aligned}\right\} \tag{15}$$

In the preceding equations, we consider

$$A_1 = \frac{\mu_{nf}}{\mu_f}, A_2 = \frac{\rho_{nf}}{\rho_f}, A_3 = \frac{\left(\rho C_p\right)_{nf}}{\left(\rho C_p\right)_f}\ A_4 = \frac{\sigma_{nf}}{\sigma_f}, A_5 = \frac{k_{nf}}{k_f}\ A_6 = \frac{\left(\rho\beta\right)_{nf}}{\left(\rho\beta\right)_f}$$

Here the radiation heat flux q_r , With higher orders disregarded, T^4 represents the temperature as a linear Taylor series T function. $T^4 \cong 4T_\infty^{\ 3}T - 3T_\infty^{\ 4}$

The following are some analytical definitions of these parameters:

$$q_r = \frac{-4\sigma^*}{3k^*}\frac{\partial T^4}{\partial y}, M = \frac{\sigma_f B_0^{\,2} 2x}{U_0 \rho_f}, Rd = \frac{4\sigma^* T_\infty^{\,3}}{3 k_f k^*}, \delta_1 = \frac{g\beta_2 \left(T_w - T_\infty\right)}{\beta_1}, Q == \frac{Q_0 2x}{\rho c_p},$$
$$\delta_2 = \frac{g\beta_2^{\,*}\left(C_w - C_\infty\right)}{\beta_1^*}, \mathrm{Re}_x = \frac{U_0 2x}{\nu}, K = \frac{2x\nu}{U_0 k_1}, Fr = \frac{2xc}{\sqrt{k_1}}, Ec = \frac{U_0^{\,2}}{c_p (T_w - T_\infty)}, \gamma = \frac{Gr_x}{\mathrm{Re}_x}, \quad (16)$$
$$Gr_x = \frac{g\beta_1 \left(T_w - T_\infty\right)\left(2x\right)^3}{\nu^2}, S = -v_w\sqrt{\frac{2x}{\nu U_0}}, Sc = \frac{\nu}{D}, \gamma_1 = \frac{2xKr}{U_0}\left(C_w - C_\infty\right)^{n-1}, \mathrm{Pr} = \frac{\mu c_p}{k}.$$

It can be done to determine the thermophoretic velocity V_T via surface mass fluxing.

$$V_T = \frac{\partial T}{\partial y} = -k\nu\frac{\nabla T}{T_r} \quad (17)$$

One expression for the thermophoretic coefficient *k* is

$$k = \frac{2C_s\left(\frac{\lambda_g}{\lambda_p} + C_t K_n\right)\left[\left(1+K_n\right)\left(C_1 + C_2 e^{-C_3/K_n}\right)\right]}{\left[\left(1+3C_m K_n\right)\left(1+2\frac{\lambda_g}{\lambda_p} + 2C_t K_n\right)\right]} \quad (18)$$

Here $C_1,\ C_2,\ \ C_3,\ \ C_m\ \ and\ C_s$ are the constants.

The thermophoretic coefficient, denoted by *k*, may take on values between $(0.2 \le k \le 1.2)$.

We may express the thermophoretic parameter as

$$\tau = -\frac{k\left(T_w - T_\infty\right)}{T_r} \quad (19)$$

3. Engineering concepts

3.1. Skin friction coefficient calculated

It is written in the following manner: $Cf_x = \frac{\tau_w}{\rho_f (U_0)^2}$. Shear stress is described in the sentence that follows.:

$$\tau_w = \mu_{nf}\left(1+\frac{1}{\beta}\right)\left(\frac{\partial u}{\partial y}\right)_{y=0} \tag{20}$$

Finally, we have

$$Cf = Cf_x \operatorname{Re}_x^{-1/2} = 2A_1\left(1+\frac{1}{\beta}\right) f''(0) \tag{21}$$

3.2. Nusselt number

As one of the basic physical quantities, heat transfer is

$$Nu_x = \frac{xq_w}{k_f\left(T_w - T_\infty\right)} \tag{22}$$

Where q_w is the surface heat flow in the x-direction, which is determined.

$$q_w = -\left(k_{nf} + \frac{16\sigma T_\infty{}^3}{3k^*}\right)\left[\frac{\partial T}{\partial y}\right]_{y=0}$$

we have

$$Nu = Nu_x \operatorname{Re}_x^{-1/2} = -\left(A_5 + Rd\right)\theta'(0) \tag{23}$$

3.3. Sherwood number

The rate of Sherwood no, which is represented as the fundamental physical quantities, is

$$Sh = \frac{J_s}{U_0 C_\infty} \tag{24}$$

Where J_s is the surface mass fluxing perceived as

$$J_s = -D\left(\frac{\partial C}{\partial y}\right)_{y=0}$$ than

we have

$$Sh = Sh_x \operatorname{Re}_x^{1/2} = -\phi'(0) \tag{25}$$

4. Numerical Approach

The governing equations are allowed to run, which converts the problem into an initial value problem. $f(\eta)=g_1,\ f'(\eta)=g_2,\ f''(\eta)=g_3,\ \ f'''(\eta)=g_3',\ \theta(\eta)=g_4,\ \theta'(\eta)=g_5,\ \theta''(\eta)=g_5',$ $\phi(\eta)=g_6,\ \phi'(\eta)=g_7,\ \phi''(\eta)=g_7'.$ then there are reduced to

$$f'''=\frac{-\left(A_2 ff''+A_6\gamma\cos\alpha\left(\theta+\delta_1\theta^2+N(\phi+\delta_1\phi^2)\right)-A_1K\ f'-A_3M\ f'-Fr\left(f'\right)^2\right)}{A_1\left(1+\frac{1}{\beta}\right)} \quad (26)$$

$$\theta''=-\frac{\left(A_4\Pr f\theta'+A_1\Pr Ec\left(1+\frac{1}{\beta}\right)f''^2+A_3\Pr EcM\left(f'\right)^2+Q\Pr\theta\right)}{\left(A_5+Rd\right)} \quad (27)$$

$$\phi''=-\left(Scf\phi'-Sc\tau\theta'\phi'-Sc\tau\phi\theta''-Sc\gamma_1\phi^n\right) \quad (28)$$

boundary conditions are

$$\left.\begin{array}{l} f'(0)=1+D_1\left(1+\frac{1}{\beta}\right)f''(0),\quad f(0)=S,\quad \theta(0)=1+D_2\,\theta'(0),\quad \phi(0)=1+D_2\,\phi'(0) \\ f'(\infty)=0,\quad \theta(\infty)=0,\quad \phi(\infty)=0. \end{array}\right\} \quad (29)$$

The equations (26)-(29) can be expressed as

$$\begin{bmatrix} g_1' \\ g_2' \\ g_3' \\ g_4' \\ g_5' \\ g_6' \\ g_7' \end{bmatrix}=\begin{bmatrix} g_2 \\ g_3 \\ \dfrac{-\left(A_2g_1g_3+A_6\gamma\cos\alpha\left(g_4+\delta_1g_4^2+N(g_6+\delta_1g_6^2)\right)-A_1K\ g_2-A_3M\ g_2-Fr\left(g_2\right)^2\right)}{A_1\left(1+\frac{1}{\beta}\right)} \\ g_5 \\ -\dfrac{\left(A_4\Pr g_1g_5+A_1\Pr Ec\left(1+\frac{1}{\beta}\right)\left(g_3\right)^2+A_3\Pr EcM\left(g_2\right)^2+Q\Pr g_4\right)}{\left(A_5+Rd\right)} \\ g_7 \\ -\left(Scg_1g_7-Sc\tau g_5g_7-Sc\tau g_6g_7'-Sc\gamma_1g_5^{\,n}\right) \end{bmatrix} \quad (30)$$

Boundary condition is

$$\left.\begin{array}{ll} g_1 = S, \quad g_2 = 1 + \left(1 + \dfrac{1}{\beta}\right) D_1 g_3,\ g_4 = 1 + D_2 g_4,\ y_6 = 1 + D_3 g_7, & at\ \ \eta = 0 \\ y_2 = 0, \quad y_4 = 0\ \ , y_6 = 0 & at\ \ \eta = \infty \end{array}\right\} \tag{31}$$

Equation (30) above uses the *MAPLE* program and R-K4th order together with the shooting technique shown in Figure 2. As a result, the leading equations are solved in equations (31), lengthwise with their boundaries. Limiting asymptotic conditions in Equation (31) $\eta \to \infty$ was revived by an imperfect set of efforts η, says η a state when there are no obvious change in Temperature, Velocity, concentration profile, and all effects parameters. This performance is generally regarded as satisfactory in the domain of boundary layer investigation. When attempting to solve an issue, step scope with $\Delta\eta = 0.01$. It's better to be realistic about the inward converging condition 10^{-6} under all circumstances.

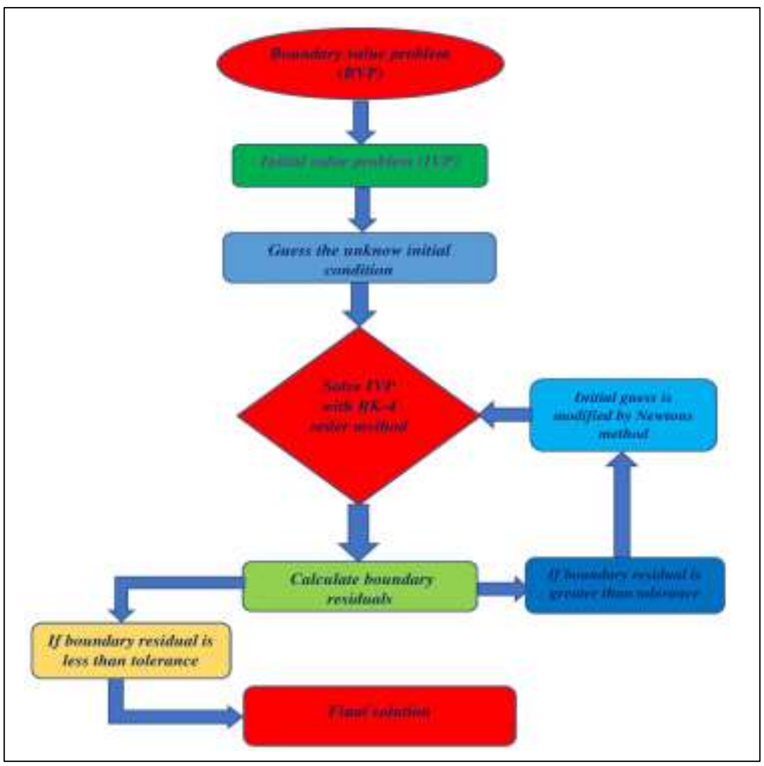

Fig. 2. Flowchart for the RK-4 Method

6. Confirmation of Results

The goal of the present study is to visualize the physical investigation of all flow parameters, their effect on nano-liquids, and their applicability in biological and medical fields. In the base fluid blood and copper nanoparticle. This investigation of mixed convection-driven Non-Darcy Forchheimer flows driven by MHD Casson nanofluid (Blood/Cu) over an inclined plate with computation of Newtonian and non-Newtonian fluids. The governing nonlinear duo PDEs are changed into ODEs by similarity transmutations, and these ODEs are then numerically (RK-4th Order) solved using the Maple software solver. The following lists have constant values for dimensionless parameters. $Rd = 0.1$, $\gamma = 1, \phi_1 = 0.0.2$, $N = 0.5, \tau = 1$, $K = 0.5$, $D_1 = 0.2, D_2 = 0.4, D_3 = 0.2, M = 1.0$, $\delta_1 = 2, \delta_2 = 0.4$, $Pr = 21$, $Ec = 0.1$, $S = 0.5$, $\gamma_1 = 1$, $Sc = 0.5$, $Fr = 0.3$, $\beta = \infty$ is non-Newtonian fluid, $\beta = 2.5$ is a Newtonian fluid, $\alpha = 90^\circ$ is the vertical plate and $\alpha = 30^\circ$ is the inclined plate is considered. The thermo-physical properties of nanoparticles are shown in Table 1. The influence of active variables, including the magnetic parameter (*M*), ($S > 0$) suction, ($S < 0$) injection, porosity (*K*), α angle of inclination, buoyancy force (γ), Non-Darcy Forchheimer (Fr), thermal radiation (*Rd*), (*N)* is the buoyancy ratio parameter, (*Pr)* Prandtl number, Sc is Schmidt number, (τ) thermophoresis parameter, (*Ec*) Eckert number on discussed $\theta(\eta)$, concentration profiles $\phi(\eta)$, velocity profiles $f'(\eta)$, Temperature profiles, Nusselt number, skin-friction, and Sherwood number for comparison of computation of Newtonian fluid and non-Newtonian fluids. Graphs are used to depict these parameters.

6.1 Profile of velocity

Figures 3-9 display the effects of the Magnetic field (*M*), porosity (*K*), α angles vertical plate, Darcy Forchheimer (Fr), and ϕ_1 volume friction on velocity $f'(\eta)$ for inclined vertical plates for computation of non-Newtonian fluid and non-Newtonian fluid. Fig 3 proves the consequence of ϕ_1 volume friction on the velocity $f'(\eta)$ over an inclined plate. As the ϕ_1 increases, the velocity $f'(\eta)$ rises across inclined plates. Fig. 4 proves the consequence of the M on the velocity $f'(\eta)$ for the comparison of Newtonian fluids and non-Newtonian fluids over an inclined

ngth rises,
rce they ge
physical ur
vertical pla
ariable (K)

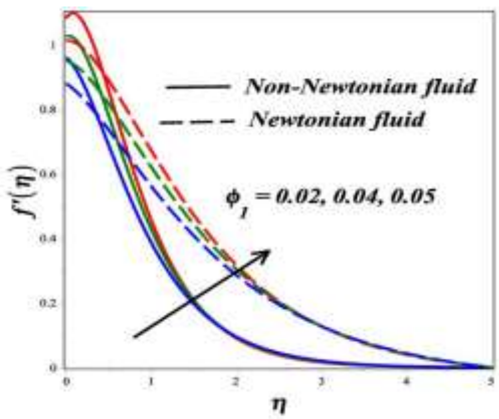

Figure **3** The consequence of ϕ_1 on the $f'(\eta)$

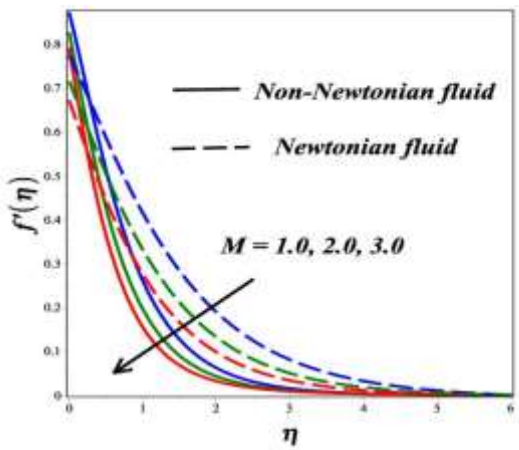

Figure **4** The consequence of M on the $f'(\eta)$

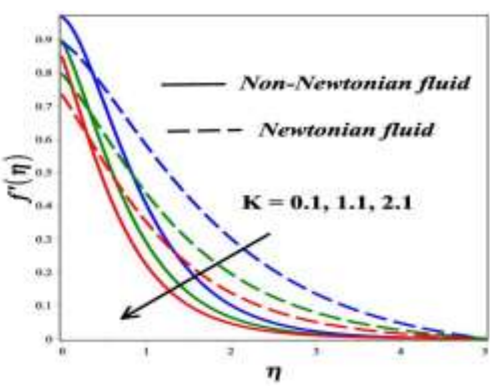

Figure **5** The consequence of K on the $f'(\eta)$

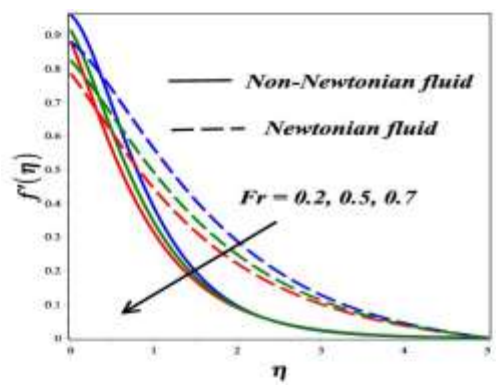

Figure **6** The consequence of Fr on the $f'(\eta)$.

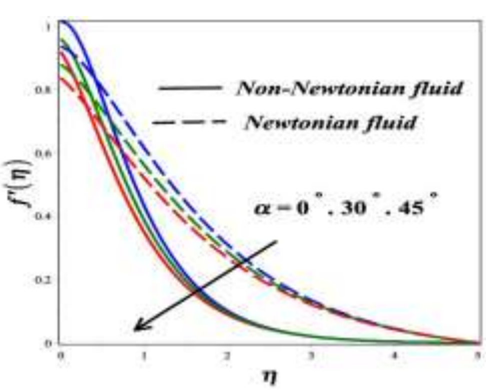

Figure **7** The consequence of α on the $f'(\eta)$.

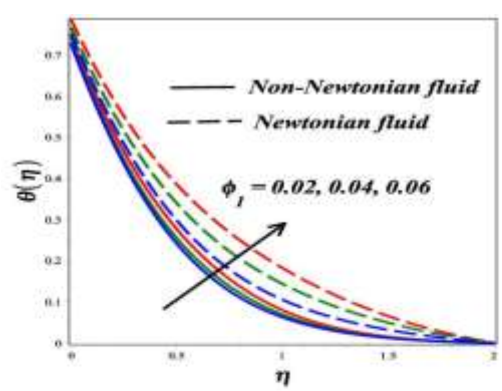

Figure **8** The consequence of ϕ_1 on the $f'(\eta)$.

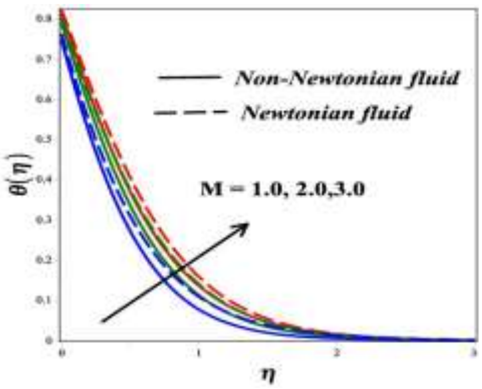

Figure **9.** The consequence of M on the $\theta(\eta)$.

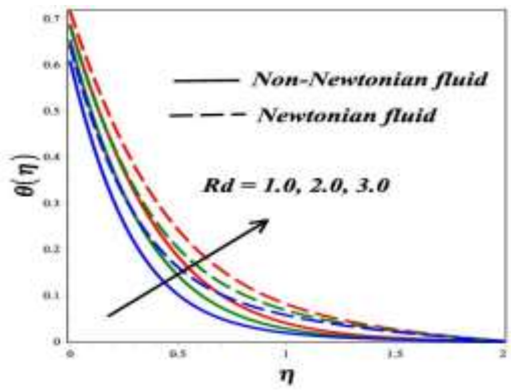

Figure **10** The consequence of Rd on the $\theta(\eta)$.

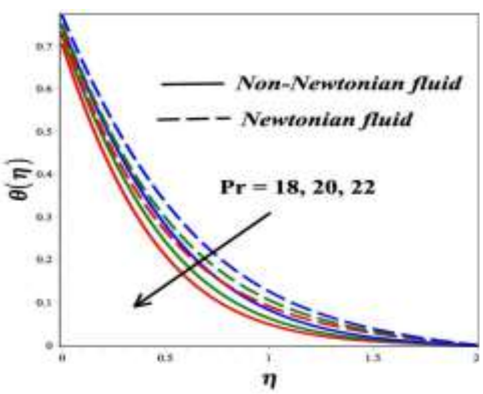

Figure **11** The consequence of Pr on the $\theta(\eta)$.

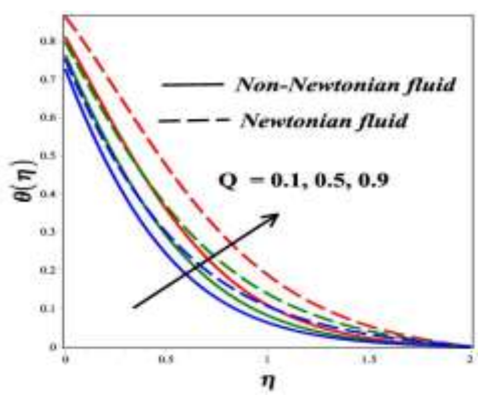

Figure **12**The consequence of Q on the $\theta(\eta)$.

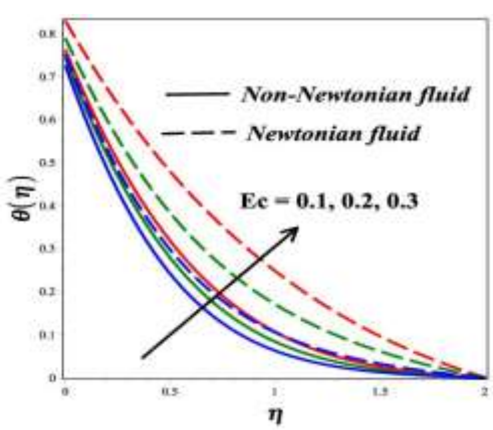

Figure **13** The consequence of Ec on the $\theta(\eta)$.

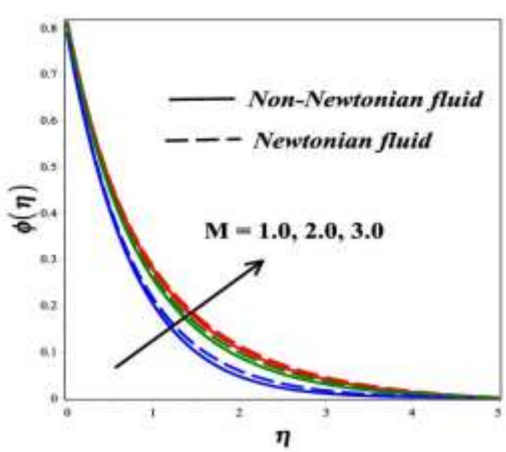

Figure **14** The consequence of M on the $\phi(\eta)$.

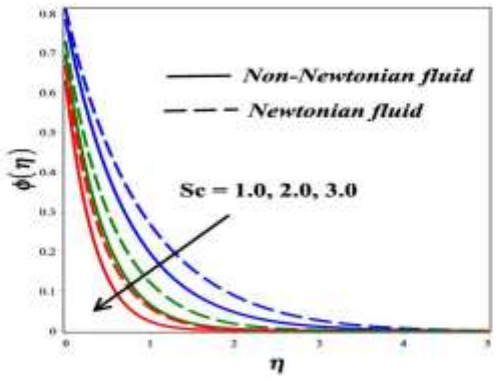

Figure **15** The consequence of Sc on the $\phi(\eta)$

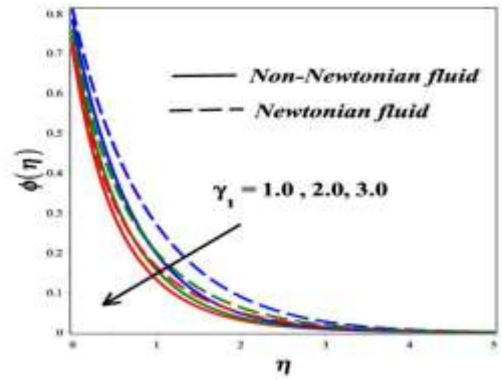

Figure **16** The consequence of γ_1 on the $\phi(\eta)$

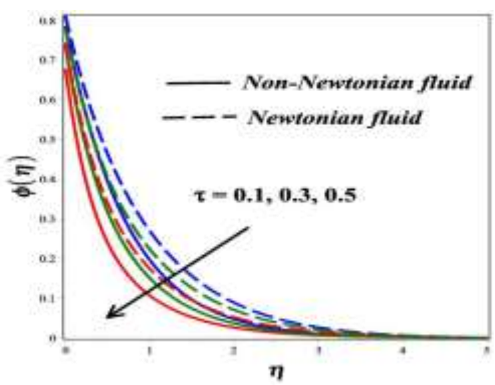

Figure **17** The consequence of τ on the $\phi(\eta)$.

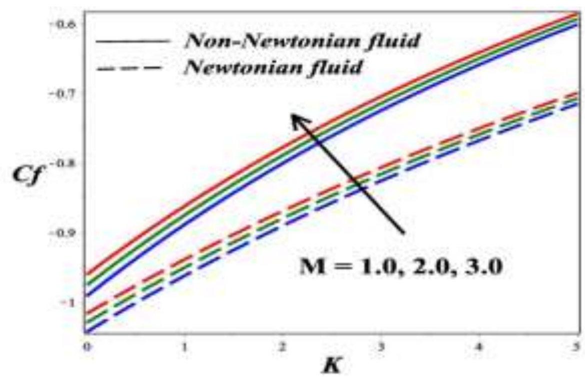

Figure **18** The consequence of K and M on the Cf

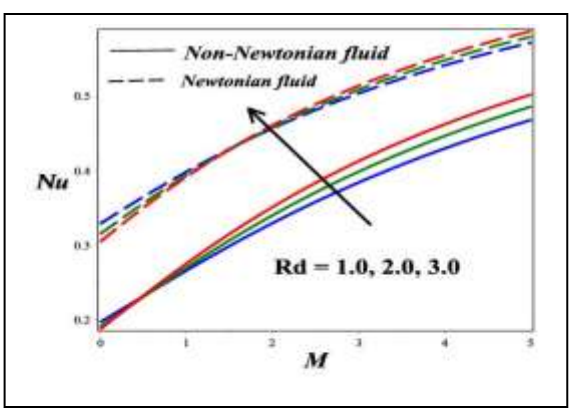

Figure **19** The consequence of Rd and M on the Nu

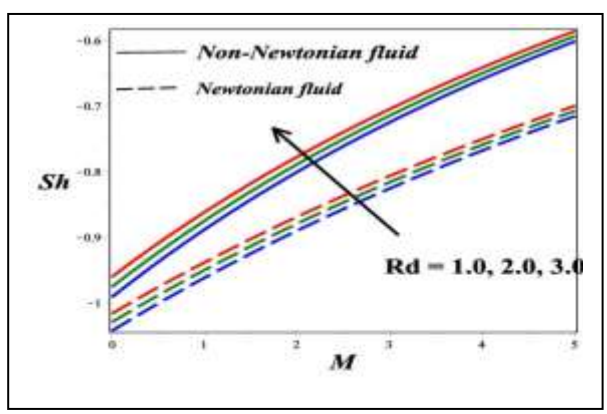

Figure **20** The consequence of Rd and M on the Sh

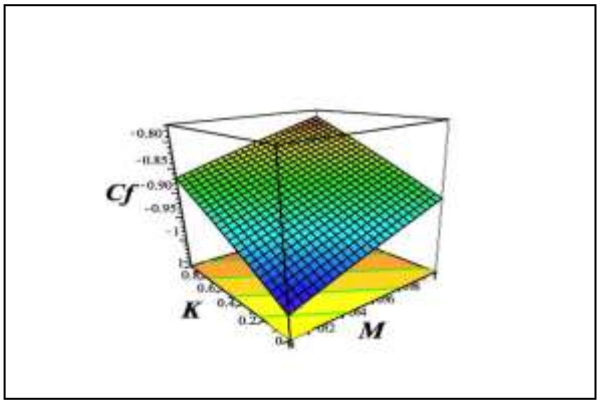

Figure **21** The consequence of M and K on the Cf for 3D

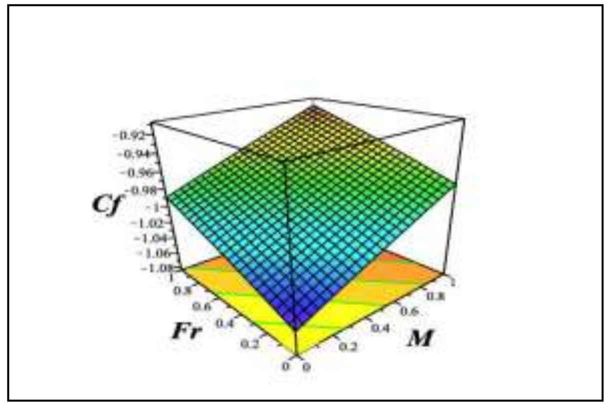

Figure **22** The consequence of M and Fr on the Cf for 3D

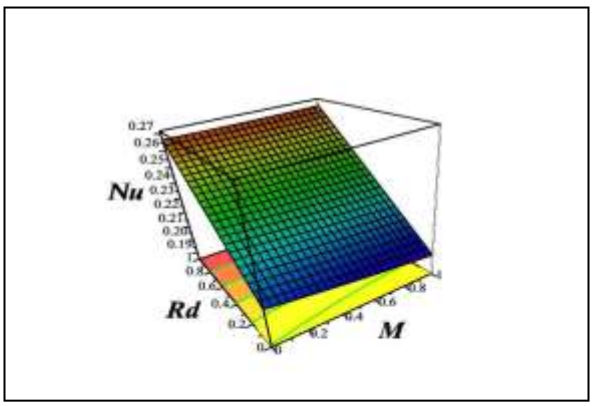

Figure **23** The consequence of Rd and M on the Nu for 3D

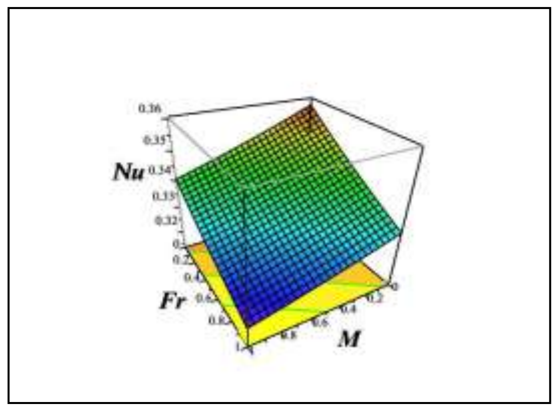

Figure **24** The consequence of Fr and M on the Nu for 3D

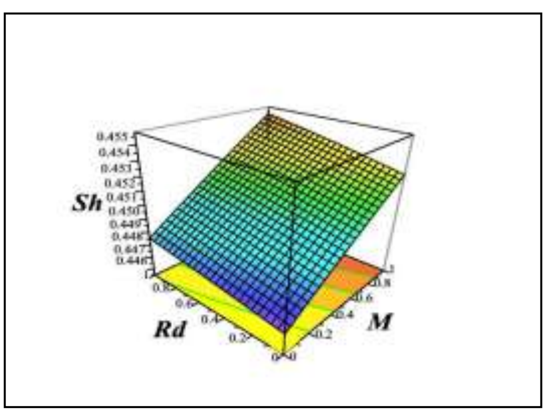

Figure **25** The consequence of Rd and M on the Sh for 3D

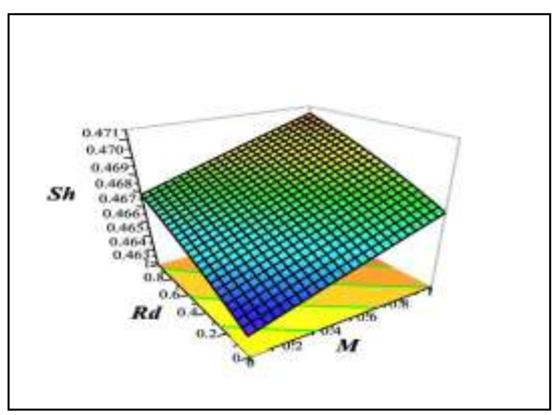

Figure **26** The consequence of Rd and M on the Sh for 3D

Fig. 6 protests the consequence of the Fr on the $f^{'}(\eta)$ for comparison of Newtonian and non-Newtonian over an inclined vertical plate. As the Darcy Forchheimer Fr rises, the $f^{'}(\eta)$ decreases across inclined vertical plates. Fig. 7 demonstrates the importance of angle (α) on the velocity $f^{'}(\eta)$ for comparison of suction and injection over an inclined vertical plate. As the α increases, the velocity profile decreases through inclined plates.

6.2 Temperature profiles

In Figures 8-13, the inclined plates on the Temperature profile $\theta(\eta)$ are shown for several influence parameters such as *M, Rd, Ec,* Q, ϕ_1, and $\Pr$. Fig. 8 shows the consequences of the (ϕ_1) temperature $\theta(\eta)$ for comparison of Newtonian and non-Newtonian fluids over inclined vertical plates. As the ϕ_1 rises, the temperature profile increases for Newtonian and non-Newtonian fluids cases. Fig. 9 establishes the consequences of the *M* on the temperature $\theta(\eta)$ for comparison of Newtonian and non-Newtonian fluids over an inclined vertical plate. The temperature across the inclined plates rises as the magnetic field intensity increases as well. Due to the Lorentz force physiologically. Fig. 10 shows the impression of *Rd* on temperature $\theta(\eta)$ over an inclined plate. The temperature profile rises as the *Rd* rises for the comparison of Newtonian and non-Newtonian over an inclined vertical plate. Physically, the fact that the radiation flux rises as the flow progresses the $\theta(\eta)$ so enhances the flow development. Fig. 11 shows the inspiration *Pr* for the temperature profile $\theta(\eta)$. As the *Pr* rises, the $\theta(\eta)$ decreases through inclined plates. Fig. 12 shows the inspiration of the Heat generation (Q) on the temperature profile $\theta(\eta)$ over inclined vertical plates. As the *Q* rises, the $\theta(\eta)$ increases through inclined plates. Figure 13 shows the inspiration of the Ec on the $\theta(\eta)$ over-inclined vertical plates. As the *Ec* rises, the $\theta(\eta)$ increases through inclined plates.

6.2 Concentration profiles

Figures 14-17 show the consequence of the γ_1 chemical reactions, Sc which is the Schmidt number, M, (τ) thermophoresis parameter on concentration profiles $\phi(\eta)$ for comparison of Newtonian and non-Newtonian cases of inclined vertical plates. Fig. 14 protests the effect of M the $\phi(\eta)$ on an inclined plate. As the M increases, the $\phi(\eta)$ profile increases across inclined plates. Fig. 15 protests the effect of Sc the $\phi(\eta)$ on an inclined plate. As the Sc Schmidt number increases, the $\phi(\eta)$ profile decreases across inclined plates. Fig. 16 shows the importance of γ_1 chemical reactions on the concentration profiles $\phi(\eta)$ across inclined plates. As the γ_1 chemical reactions increase, the $\phi(\eta)$ increase across inclined plates. Fig. 17 illustrates the outcome of τ the thermophoresis parameter on concentration profiles $\phi(\eta)$ over an inclined plate. As the τ thermophoresis increases, the $\phi(\eta)$ profile decreases in both cases Newtonian and non-Newtonian fluids across inclined plates. Since the thermophoresis effect reduces the thermal boundary layer, this also means that the concentration boundary layer thickens as the rate of the effect rises.

The impression of *K* and *M* on skin friction $Cf_x \operatorname{Re}_x^{-1/2}$ Casson nanofluid over an inclined plate is seen in Figure 18. Observing the effect of the $Cf_x \operatorname{Re}_x^{-1/2}$ many values of K *and M* is haggard. This has been observed to be the case $Cf_x \operatorname{Re}_x^{-1/2}$ in an increase in two fluids. The impression of *Rd* and *M* on the $Nu_x \operatorname{Re}_x^{-1/2}$ Casson nanofluid over an inclined plate is seen in Figure 19. Observing the effect of the $Nu_x \operatorname{Re}_x^{-1/2}$ many values of *Rd, and M* is haggard. This has been observed to be the case $Nu_x \operatorname{Re}_x^{-1/2}$ in a rising function with Rd and *M* growing for inclined plates. The impression of *Rd* and *M* on the Sherwood number $Sh_x \operatorname{Re}_x^{-1/2}$ for Casson nanofluid over an inclined plate is got in Figure 20. Observing the consequence of the $Sh_x \operatorname{Re}_x^{-1/2}$ many values of *Rd and M* is worn. This has been observed to be the case $Sh_x \operatorname{Re}_x^{-1/2}$ for Newtonian and non-Newtonian fluids is a rising function with Rd and *M* growing for inclined plates.

The impression of *K* and *M* on skin friction $Cf_x \operatorname{Re}_x^{-1/2}$ Casson nanofluid over an inclined plate for 3D diagrams is seen in Fig 21. The impression of *Fr* and *M* on skin friction $Cf_x \operatorname{Re}_x^{-1/2}$ Casson nanofluid over an inclined plate for 3D diagrams is seen in Fig 22. The impression of *Rd* and *M* on skin friction $Nu_x \operatorname{Re}_x^{-1/2}$ Casson nanofluid over an inclined plate for 3D diagrams is seen in Fig 23. The impression of *Fr* and *M* on skin friction $Nu_x \operatorname{Re}_x^{-1/2}$ Casson nanofluid over an inclined plate for 3D diagrams is seen in Fig 24. The impression of *Rd* and *M* on skin friction $Sh_x \operatorname{Re}_x^{-1/2}$ Casson nanofluid over an inclined plate for 3D diagrams is seen in Fig 25. The impression of γ_1 and M on skin friction $Sh_x \operatorname{Re}_x^{-1/2}$ Casson nanofluid over an inclined plate for 3D diagrams is seen in Fig 26. We find excellent agreement when Table 2 compares the assessment with previously published results for the following researchers: Mills et al. [36], Tsai [37] and Alam et al. [38], and Jha and Samaila [32].

Table 1 Nanoparticle thermophysical characteristics: Dolui *et al*. [39].

Property	Blood (b_f)	**Copper** (Cu)
$\rho\left(kg/m^3\right)$	1063	**8933**
$c_p\ (J/kgK)$	3594	385
$k\ (W/mk)$	0.492	401
$\sigma(s/m)$	0.667	59.6×10^6
$\beta\times10^{-6}\left(K^{-1}\right)$	1.8	16.7
Pr	21	-

Table.2 A comparison of Stanton numbers in some literature such consider the values $Sc = 1000, M = Ec = \delta_1 = \delta_2 = 0 \textit{ and } \alpha = 90^\circ$.

τ	S	**Mills et al.** [36]	**Tsai** [37]	**Alam et al.** [38]	**Jha and Samaila** [32]	**Present results**
1	1	0.8619	0.9134	0.8691	0.8693	0.86830
1	0.5	0.5346	0.5598	0.5359	0.5368	0.53582
1	0.0	0.2095	0.2063	0.2076	0.2081	0.20714
1	-0.004	0.2068	0.2034	0.2070	0.2089	0.20853
1	-0.005	0.2062	0.2027	0.2065	0.2073	0.20716
1	-0.25	0.0344	0.0295	0.0349	0.0359	0.03529

7. Conclusions

This study employs MHD Casson nanofluid (Blood/Cu) buoyancy-driven mixed convection slips flow over a porous inclined plate with chemical reactions and also compares to Newtonian and non-Newtonian. The governing nonlinear coupled PDEs are converted into ODEs via similarity transformations. The NM is used in the MAPLE software to compute the graphical results of the flow parameters. The effects of temperature, velocity, concentration, heat transfer, skin friction coefficients, and Sherwood number on physical restrictions like a magnetic field, porosity, buoyancy force and buoyancy ratio parameter, thermal radiation, chemical reactions, Schmidt number, and thermophoresis are discussed through graphs. It has many applications, such as aerodynamic extrusion of plastic sheets, including die-extruded polymer sheets, glass-blowing-spun fibers, continuous casting, and biomedical uses in antimicrobial agents, diagnostic, and drug delivery. Here we explain the key findings of the study,

- ❖ The velocity profile decreases for Newtonian and non-Newtonian fluids over inclined plates while the porosity and magnetic field parameters increase.
- ❖ As the morals of the thermal radiation, magnetic field, and volume friction increase, the temperature increases in Newtonian and non-Newtonian fluids.
- ❖ As the chemical reaction parameters rise, inclined plate concentration profiles decrease for Newtonian and non-Newtonian fluids.
- ❖ As the Schmidt number and thermophoresis parameters rise, inclined plate concentration profiles decrease for Newtonian and non-Newtonian fluids.
- ❖ As skin friction across an inclined plate increases, the impression of K and M values rises.
- ❖ The impression of *Ec*, *Rd*, and *M* values grows as the Skin friction, Nusselt number, and Sherwood number over an inclined plate for 3D graphs.

NOMENCLATURE			
A	Constant	β	Casson fluid parameter
B_0	Magnetic field induction	**Greek symbols**	
D_1	Velocity slip	T	Temperature at the surface
D_2	Temperature slip	T_W	Surface Temperature
D_2	Mass slip	T_∞	Ambient Fluid temperature
$Cf_x \operatorname{Re}_x^{-1/2}$	skin friction	v_w	Transpiration velocity
c_p	Specific heat	x, y	Axis in the direction along and normal to the plate
C_1, C_2, C_3	Constants	ρ	Fluid density
Ec	Eckert number	β	Casson fluid parameter
Gr_x	Local Grashof number	μ	Fluid dynamic viscosity
g	Acceleration due to gravity	α_1	Temperature ratio parameter

k	Thermal conductivity	α_2	concentration ratio parameter
K	Porosity parameter	β_1, β_2	Thermal expansion coefficient for temperature
N	Buoyancy ratio parameter	β_1^*, β_2^*	Thermal expansion coefficient for concentration
M	Magnetic parameter	ν	Kinetic viscosity
$Nu_x \mathrm{Re}_x^{-1/2}$	Nusselt number	σ	Electrical conductivity
Pr	Prandtl number	θ	The dimensionless Temperature of a fluid
q_r	Radiative heat flux	ψ	Steam function
q_w	Surface heat flux	τ_w	Wall shear stress
Fr	Darcy Forchheimer	η	Similarity variable
Q	Heat source	σ^*	Stefan-Boltzmann constant
Re_x	Local Reynolds number	γ	Local buoyancy parameter
Rd	Thermal Radiation parameter	λ_1	Heat generation parameter
S	Suction / Injection parameter	k^*	Mean absorption coefficient
Sc	Schmidt number	γ_1	Chemical reaction parameters.

References:

[1] S. U. S. Choi, "Enhancing thermal conductivity of fluids with nanoparticles," *Am. Soc. Mech. Eng. Fluids Eng. Div. FED*, vol. 231, no. March, pp. 99–105, 1995.

[2] N. Ahmed, N. A. Shah, B. Ahmad, S. I. A. Shah, S. Ulhaq, and M. Rahimi-Gorji, "Transient MHD convective flow of fractional nanofluid between vertical plates," *J. Appl. Comput. Mech.*, vol. 5, no. 4, pp. 592–602, 2019, doi: 10.22055/JACM.2018.26947.1364.

[3] I. Khan, "New idea of Atangana and Baleanu fractional derivatives to human blood flow in nanofluids," *Chaos*, vol. 29, no. 1, 2019, doi: 10.1063/1.5078738.

[4] T. Hayat, S. Qayyum, A. Alsaedi, and B. Ahmad, "Entropy generation minimization: Darcy-Forchheimer nanofluid flow due to curved stretching sheet with partial slip," *Int. Commun. Heat Mass Transf.*, vol. 111, p. 104445, 2020, doi: 10.1016/j.icheatmasstransfer.2019.104445.

[5] U. Khan, A. Zaib, S. Abu Bakar, and A. Ishak, "Stagnation-point flow of a hybrid nanoliquid over a non-isothermal stretching/shrinking sheet with characteristics of inertial and microstructure," *Case Stud. Therm. Eng.*, vol. 26, no. June, p. 101150, 2021, doi: 10.1016/j.csite.2021.101150.

[6] I. A. Badruddin, Z. A. Zainal, P. A. A. Narayana, K. N. Seetharamu, and L. W. Siew, "Free convection and radiation characteristics for a vertical plate embedded in a porous medium," *Int. J. Numer. Methods Eng.*, vol. 65, no. 13, pp. 2265–2278, 2006, doi: 10.1002/nme.1541.

[7] M. G. Reddy, M. V. V. N. L. Sudharani, and K. G. Kumar, "An analysis of dusty slip flow through a single-/multi-wall carbon nanotube," *Contin. Mech. Thermodyn.*, vol. 32, no. 3, pp. 971–985, 2020, doi: 10.1007/s00161-019-00860-5.

[8] D. V. K. Prasad, G. S. K. Chaitanya, and R. S. Raju, "Double diffusive effects on mixed convection Casson fluid flow past a wavy inclined plate in presence of Darcian porous medium," *Results Eng.*, vol. 3, no. April, p. 100019, 2019, doi: 10.1016/j.rineng.2019.100019.

[9] S. Bilal, K. K. Asogwa, H. Alotaibi, M. Y. Malik, and I. Khan, "Analytical treatment of radiative Casson fluid over an isothermal inclined Riga surface with aspects of chemically reactive species," *Alexandria Eng. J.*, vol. 60, no. 5, pp. 4243–4253, 2021, doi: 10.1016/j.aej.2021.03.015.

[10] X. Qiang, I. Siddique, K. Sadiq, and N. A. Shah, "Double diffusive MHD convective flows of a viscous fluid under influence of the inclined magnetic field, source/sink and chemical reaction," *Alexandria Eng. J.*, vol. 59, no. 6, pp. 4171–4181, 2020, doi: 10.1016/j.aej.2020.07.023.

[11] K. Raghunath, "Study of Heat and Mass Transfer of an Unsteady Magnetohydrodynamic (MHD) Nanofluid Flow Past a Vertical Porous Plate in the Presence of Chemical Reaction, Radiation and Soret Effects," *J. Nanofluids*, vol. 12, no. 3, pp. 767–776, 2023, doi: 10.1166/jon.2023.1965.

[12] P. Sudarsana Reddy, A. J. Chamkha, and A. Al-Mudhaf, "MHD heat and mass transfer flow of a nanofluid over an inclined vertical porous plate with radiation and heat generation/absorption," *Adv. Powder Technol.*, vol. 28, no. 3, pp. 1008–1017, 2017, doi: 10.1016/j.apt.2017.01.005.

[13] M. Goyal and R. Bhargava, "Simulation of Natural Convective Boundary Layer Flow of a Nanofluid Past a Convectively Heated Inclined Plate in the Presence of Magnetic Field," *Int. J. Appl. Comput. Math.*, vol. 4, no. 2, pp. 1–24, 2018, doi: 10.1007/s40819-018-0483-0.

[14] A. Rauf, N. Ali Shah, A. Mushtaq, and T. Botmart, "Heat transport and magnetohydrodynamic hybrid micropolar ferrofluid flow over a non-linearly stretching sheet," *AIMS Math.*, vol. 8, no. 1, pp. 164–193, 2023, doi: 10.3934/math.2023008.

[15] N. Abbas, W. Shatanawi, and T. A. M. shatnawi, "Thermodynamic study of radiative chemically reactive flow of induced MHD sutterby nanofluid over a nonlinear stretching cylinder," *Alexandria Eng. J.*, vol. 70, pp. 179–189, 2023, doi: 10.1016/j.aej.2023.02.038.

[16] K. Ahmed, T. Akbar, I. Ahmed, T. Muhammad, and M. Amjad, "Mixed convective MHD flow of Williamson fluid over a nonlinear stretching curved surface with variable thermal conductivity and activation energy," *Numer. Heat Transf. Part A Appl.*, vol. 0, no. 0, pp. 1–16, 2023, doi: 10.1080/10407782.2023.2194689.

[17] K. Sakkaravarthi and P. B. A. Reddy, "Entropy optimization of MHD hybrid nanofluid flow through a curved stretching sheet with thermal radiation and heat generation: Semi-

analytical and numerical simulations," *Proc. Inst. Mech. Eng. Part E J. Process Mech. Eng.*, pp. 1–11, 2022, doi: 10.1177/09544089221100222.

[18] M. Qayyum *et al.*, "Heat Transfer Analysis of Unsteady MHD Carreau Fluid Flow over a Stretching/Shrinking Sheet," *Coatings*, vol. 12, no. 11, 2022, doi: 10.3390/coatings12111661.

[19] M. Y. Ali, S. Reza-E-Rabbi, M. M. H. Rasel, and S. F. Ahmmed, "Combined impacts of thermoelectric and radiation on hydromagnetic nanofluid flow over a nonlinear stretching sheet," *Partial Differ. Equations Appl. Math.*, vol. 7, no. February, p. 100500, 2023, doi: 10.1016/j.padiff.2023.100500.

[20] B. Ali, A. Shafiq, I. Siddique, Q. Al-Mdallal, and F. Jarad, "Significance of suction/injection, gravity modulation, thermal radiation, and magnetohydrodynamic on dynamics of micropolar fluid subject to an inclined sheet via finite element approach," *Case Stud. Therm. Eng.*, vol. 28, no. October, p. 101537, 2021, doi: 10.1016/j.csite.2021.101537.

[21] N. Gulle and R. Kodi, "Soret radiation and chemical reaction effect on MHD Jeffrey fluid flow past an inclined vertical plate embedded in porous medium," *Mater. Today Proc.*, vol. 50, pp. 2218–2226, 2021, doi: 10.1016/j.matpr.2021.09.480.

[22] P. Maghsoudi, G. Shahriari, H. Rasam, and S. Sadeghi, "Flow and natural convection heat transfer characteristics of non-Newtonian nanofluid flow bounded by two infinite vertical flat plates in presence of magnetic field and thermal radiation using Galerkin method," *J. Cent. South Univ.*, vol. 26, no. 5, pp. 1294–1305, 2019, doi: 10.1007/s11771-019-4088-5.

[23] Y. M. Chu *et al.*, "Thermal impact of hybrid nanofluid due to inclined oscillatory porous surface with thermo-diffusion features," *Case Stud. Therm. Eng.*, vol. 42, no. December 2022, p. 102695, 2023, doi: 10.1016/j.csite.2023.102695.

[24] B. Ahmad, M. Ozair Ahmad, M. Farman, A. Akgül, and M. B. Riaz, "A significance of multi slip condition for inclined MHD nano-fluid flow with non linear thermal radiations, Dufuor and Sorrot, and chemically reactive bio-convection effect," *South African J. Chem. Eng.*, vol. 43, no. September 2022, pp. 135–145, 2023, doi: 10.1016/j.sajce.2022.10.009.

[25] B. V. Swarnalathamma, D. M. P. Babu, and M. V. Krishna, "Combined impacts of Radiation absorption and Chemically reacting on MHD Free Convective Casson fluid flow past an infinite vertical inclined porous plate," *J. Comput. Math. Data Sci.*, vol. 5, no. November, p. 100069, 2022, doi: 10.1016/j.jcmds.2022.100069.

[26] R. N. Barik and G. C. Dash, "Thermal radiation effect on an unsteady magnetohydrodynamic flow past inclined porous heated plate in the presence of chemical reaction and viscous dissipation," *Appl. Math. Comput.*, vol. 226, pp. 423–434, 2014, doi: 10.1016/j.amc.2013.09.077.

[27] K. Sakkaravarthi and P. B. A. Reddy, "Entropy generation on Casson hybrid nanofluid over a curved stretching sheet with convective boundary condition: Semi-analytical and numerical simulations," *Proc. Inst. Mech. Eng. Part C J. Mech. Eng. Sci.*, 2022, doi: 10.1177/09544062221119055.

[28] A. Nayan, N. I. F. A. Fauzan, M. R. Ilias, S. F. Zakaria, and N. H. Z. Aznam, "Aligned Magnetohydrodynamics (MHD) Flow of Hybrid Nanofluid Over a Vertical Plate Through Porous Medium," *J. Adv. Res. Fluid Mech. Therm. Sci.*, vol. 92, no. 1, pp. 51–64, 2022, doi: 10.37934/arfmts.92.1.5164.

[29] D. Sarma and K. K. Pandit, "Effects of Hall current, rotation and Soret effects on MHD free convection heat and mass transfer flow past an accelerated vertical plate through a porous medium," *Ain Shams Eng. J.*, vol. 9, no. 4, pp. 631–646, 2018, doi: 10.1016/j.asej.2016.03.005.

[30] G. Revathi, J. B. Macherla, C. S. Raju, R. Sharma, and A. J. Chamkha, "Significance of magnetic field on Carreau dissipative flow over a curved porous surface with activation energy," *J. Nanofluids*, vol. 10, no. 1, pp. 75–82, 2021, doi: 10.1166/JON.2021.1768.

[31] S. Mukhopadhyay and G. C. Layek, "Effects of thermal radiation and variable fluid viscosity on free convective flow and heat transfer past a porous stretching surface," *Int. J. Heat Mass Transf.*, vol. 51, no. 9–10, pp. 2167–2178, May 2008, doi: 10.1016/j.ijheatmasstransfer.2007.11.038.

[32] B. K. Jha and G. Samaila, "Numerical Heat Transfer , Part B : Fundamentals Nonlinear approximation for buoyancy-driven mixed convection heat and mass transfer flow over an inclined porous plate with Joule heating , nonlinear thermal radiation , viscous dissipation , and thermophore," *Numer. Heat Transf. Part B Fundam.*, vol. 83, no. 4, pp. 139–161, 2023, doi: 10.1080/10407790.2022.2150341.

[33] A. Selim, M. A. Hossain, and D. A. S. Rees, "The effect of surface mass transfer on mixed convection flow past a heated vertical flat permeable plate with thermophoresis," *Int. J. Therm. Sci.*, vol. 42, no. 10, pp. 973–982, 2003, doi: 10.1016/S1290-0729(03)00075-9.

[34] M. S. Alam, M. M. Rahman, and M. A. Sattar, "Effects of variable suction and thermophoresis on steady MHD combined free-forced convective heat and mass transfer flow over a semi-infinite permeable inclined plate in the presence of thermal radiation," *Int. J. Therm. Sci.*, vol. 47, no. 6, pp. 758–765, 2008, doi: 10.1016/j.ijthermalsci.2007.06.006.

[35] M. V. Krishna, "Chemical reaction, heat absorption and Newtonian heating on MHD free convective Casson hybrid nanofluids past an infinite oscillating vertical porous plate," *Int. Commun. Heat Mass Transf.*, vol. 138, no. August, p. 106327, 2022, doi: 10.1016/j.icheatmasstransfer.2022.106327.

[36] A. F. Mills, H. Xu, and F. Ayazi, "The effect of wall suction and thermophoresis on aerosol particle deposition from a laminar boundary layer on a flat plate," *Int. J. Heat Mass Transf.*, vol. 27, no. 7, pp. 1110–1113, 1984, doi: 10.1016/0017-9310(84)90127-3.

[37] R. Tsai, "A simple approach for evaluating the effect of wall suction and thermophoresis on aerosol particle deposition from a laminar flow over a flat plate," *Int. Commun. Heat Mass Transf.*, vol. 26, no. 2, pp. 249–257, 1999, doi: 10.1016/S0735-1933(99)00011-1.

[38] M. S. Alam, M. M. Rahman, and M. A. Sattar, "On the effectiveness of viscous dissipation and Joule heating on steady Magnetohydrodynamic heat and mass transfer flow over an

inclined radiate isothermal permeable surface in the presence of thermophoresis," *Commun. Nonlinear Sci. Numer. Simul.*, vol. 14, no. 5, pp. 2132–2143, 2009, doi: 10.1016/j.cnsns.2008.06.008.

[39] S. Dolui, B. Bhaumik, and S. De, "Combined effect of induced magnetic field and thermal radiation on ternary hybrid nanofluid flow through an inclined catheterized artery with multiple stenosis," *Chem. Phys. Lett.*, vol. 811, no. September 2022, p. 140209, 2023, doi: 10.1016/j.cplett.2022.140209.